WASP-166b: a bloated super-Neptune transiting a $V = 9$ star

Coel Hellier,[1]★ D. R. Anderson [1], A. H. M. J. Triaud,[2,3] F. Bouchy,[2] A. Burdanov,[4] A. Collier Cameron [5], L. Delrez [4,6], D. Ehrenreich,[2] M. Gillon,[4] E. Jehin,[4] M. Lendl [2,7], E. Linder,[8] L. D. Nielsen,[2] P. F. L. Maxted,[1] F. Pepe,[2] D. Pollacco,[9] D. Queloz,[6] D. Ségransan,[2] B. Smalley [1], J. J. Spake,[10] L. Y. Temple,[1] S. Udry,[2] R. G. West [9] and A. Wyttenbach[11]

[1]*Astrophysics Group, Keele University, Staffordshire ST5 5BG, UK*
[2]*Observatoire astronomique de l'Université de Genève 51 ch. des Maillettes, CH-1290 Sauverny, Switzerland*
[3]*School of Physics & Astronomy, University of Birmingham, Edgbaston, Birmingham B15 2TT, UK*
[4]*Space sciences, Technologies and Astrophysics Research (STAR) Institute, Université de Liège, Allée du 6 Août, 17, Bat. B5C, B-4000 Liège, Belgium*
[5]*SUPA, School of Physics and Astronomy, University of St. Andrews, North Haugh, Fife KY16 9SS, UK*
[6]*Cavendish Laboratory, J J Thomson Avenue, Cambridge CB3 0HE, UK*
[7]*Space Research Institute, Austrian Academy of Sciences, Schmiedlstr 6, A-8042 Graz, Austria*
[8]*Physikalisches Institut, University of Bern, Sidlerstrasse 5, CH-3012 Bern, Switzerland*
[9]*Department of Physics, University of Warwick, Gibbet Hill Road, Coventry CV4 7AL, UK*
[10]*Astrophysics Group, School of Physics, University of Exeter, Stocker Road, Exeter EX4 4QL, UK*
[11]*Leiden Observatory, Leiden University, Postbus 9513, NL-2300 RA Leiden, the Netherlands*

ABSTRACT

We report the discovery of WASP-166b, a super-Neptune planet with a mass of 0.1 $M_{\rm Jup}$ (1.9 $M_{\rm Nep}$) and a bloated radius of 0.63 $R_{\rm Jup}$. It transits a $V = 9.36$, F9V star in a 5.44-d orbit that is aligned with the stellar rotation axis (sky-projected obliquity angle $\lambda = 3 \pm 5$ deg). Variations in the radial-velocity measurements are likely the result of magnetic activity over a 12-d stellar rotation period. WASP-166b appears to be a rare object within the 'Neptune desert'.

Key words: stars: individual: (WASP-166).

1 INTRODUCTION

Planets with low surface gravities have the largest atmospheric scale heights and so are the best targets for atmospheric characterization by the technique of transmission spectroscopy, in which the planet's atmosphere is projected against the host-star photosphere during transit. Having a bloated radius also means that planets of sub-Saturn mass can still produce deep-enough transits to be found in ground-based surveys. Thus discoveries such as WASP-107b (0.12 $M_{\rm Jup}$; 0.94 $R_{\rm Jup}$; Anderson et al. 2017) and WASP-127b (0.18 $M_{\rm Jup}$; 1.37 $R_{\rm Jup}$; Lam et al. 2017) are prime targets for characterization (e.g. Palle et al. 2017; Chen et al. 2018; Kreidberg et al. 2018; Spake et al. 2018). The importance of such targets, particularly ones transiting bright stars, will increase further with the launch of the *James Webb Space Telescope*.

Planets between the masses of Neptune and Saturn are transitional between ice giants and gaseous giants, and so could help to elucidate why some proto-planets undergo runaway gaseous accretion while others do not. There are also far fewer Neptune-mass systems known, compared to the abundance of super-Earths found by the Kepler mission, and the several-hundred transiting hot Jupiters now found by the ground-based surveys. The absence of Neptunes is particularly pronounced at short orbital periods, leading to the discussion of a 'Neptune desert' (Mazeh, Holczer & Faigler 2016).

Here we report the discovery of WASP-166b, the lowest mass planet yet found by the WASP survey, at only twice the mass of Neptune.

2 OBSERVATIONS

From 2006 to 2012 WASP-South operated as an array of eight cameras based on 200-mm, f/1.8 Canon lenses backed by 2k × 2k Peltier-cooled CCDs (see Pollacco et al. 2006 for an account of the WASP project). Each field was observed with typically 10-min cadence. The data were processed into a magnitude for each catalogued star, and the resulting light curves accumulated in a central archive. This was then searched for transit signals, with the best candidates sent for follow-up with the TRAPPIST-South photometer (Gillon et al. 2013) and the Euler/CORALIE spectrograph (Triaud et al. 2013). This combination has resulted in many discoveries of transiting exoplanets (e.g. Hellier et al. 2018) and the techniques and methods used here are continuations of those from previous papers.

★ E-mail: c.hellier@keele.ac.uk

Table 1. Observations of WASP-166.

Facility	Date	Notes
WASP-South	2006 May–2012 May	33 400 points
CORALIE	2014 Feb–2017 Jan	41 RVs
HARPS (orbit)	2016 Apr–2018 Mar	27 RVs
HARPS (transit)	2017 Jan 14	75 RVs
HARPS (transit)	2017 Mar 04	52 RVs
HARPS (transit)	2017 Mar 15	66 RVs
TRAPPIST-South	2014 Mar 05	z band
EulerCAM	2016 Feb 05	I_c band
TRAPPIST-South	2016 Feb 16	z' band
TESS	2019 Feb 2–27	3 transits

WASP-166 was adopted as a candidate in 2014, after detection of a 5.44-d transit signal. Radial-velocity (RV) observations with CORALIE found orbital motion at the transit period, but also showed additional variations. We thus accumulated more RV data than is usual for WASP planet discoveries in order to look for additional bodies or a longer term trend. This amounted to 41 RVs with 1.2-m Euler/CORALIE over a three-year period, and 220 RVs with the ESO 3.6-m/HARPS, of which 27 covered the orbit, while 75, 52, and 66 were taken in sequences covering transits on three different nights. The CORALIE and HARPS data were reduced using standard pipelines, as described in Rickman et al. (2019), Udry et al. (2019), and references therein.

Further photometric observations (listed in Table 1) include two partial transit light curves from TRAPPIST-South (one ingress and one egress) and a full transit from EulerCAM (Lendl et al. 2012), which unfortunately has excess red noise owing to poor observing conditions.

In 2019 February, after completion of the initial version of this paper, the TESS satellite observed the sky sector that includes WASP-166. TESS (Ricker et al. 2016) is performing an all-sky transit survey aimed primarily at rocky planets too small to be found by the ground-based surveys. It has four cameras, each with a 10-cm lens backed by four 2048×2048 CCDs covering a field of $24° \times 24°$, and observing in a bandpass from 600 to 1000 nm.

We downloaded the public TESS light curve for WASP-166 (=TIC 408310006 = TOI-576) from the Mikulski Archive for Space Telescopes (MAST). We used the standard aperture-photometry data products, and extracted sections of the data around the known transit times. Three transits were observed over the 25-d period (a fourth was recorded shortly after recovery from a data gap, and we discard it owing to strong out-of-transit variability).

3 SPECTRAL ANALYSIS

For a spectral analysis of the host star we combined and added the HARPS spectra and adopted the methods of Doyle et al. (2013). The resulting parameters are listed in Table 2. The effective temperature, $T_{\text{eff}} = 6050 \pm 50$ K, comes from the Hα line, and suggests a spectral type of F9. The surface gravity, $\log g = 4.5 \pm 0.1$ comes from Na I D and Mg I b lines. The metallicity value of [Fe/H] $= +0.19 \pm 0.05$ comes from equivalent-width measurements of unblended Fe I lines. The Fe I lines were also used to estimate a rotation speed of $v\sin i = 4.6 \pm 0.8$ km s^{-1}, after convolving with the HARPS instrumental resolution ($R = 120\,000$), and also accounting for an estimate of the macroturbulence take from Doyle et al. (2014). We also report a value for the lithium abundance of log A(Li) $= 2.68 \pm 0.08$.

Table 2. System parameters for WASP-166.

1SWASP J093930.08−205856.8
2MASS 09393009−2058568 BD−20 2976
RA $= 09^h39^m30\overset{s}{.}09$, Dec. $= -20°58'56.9''$ (J2000)
V mag $= 9.36$; *Gaia* $G = 9.26$; $J = 8.35$
Rotational modulation: <1 mmag
Gaia DR2 pm (RA) –55.082 $\pm$ 0.072 (Dec.) 10.927 $\pm$ 0.069 mas yr^{-1}
Gaia DR2 parallax: 8.7301 $\pm$ 0.0448 mas
Distance $= 113 \pm 1$ pc

Stellar parameters from spectroscopic analysis.

Spectral type	F9V
T_{eff} (K)	6050 ± 50
$\log g$	4.5 ± 0.1
$v \sin i$ (km s^{-1})	4.6 ± 0.8
[Fe/H]	$+ 0.19 \pm 0.05$
log A(Li)	2.68 ± 0.08
Age (BAGEMASS) (Gyr)	2.1 ± 0.9

Parameters from MCMC analysis (fitted parameters denoted †).

P (d)†	5.443540 ± 0.000004
T_c (TDB)†	245 7664.3289 ± 0.0006
T_{14} (d)†	0.150 ± 0.001
$T_{12} = T_{34}$ (d)	0.0088 ± 0.0012
$\Delta F^\dagger = R_P^2/R_*^2$	0.00281 ± 0.00007
b†	0.39 ± 0.10
i (°)	88.0 ± 0.7
K_1 (km s^{-1})†	0.0104 ± 0.0004
γ (km s^{-1})†	23.6285 ± 0.0003
e	0 (adopted) (< 0.07 at 2σ)
a/R_*	11.3 ± 0.6
M_* (M$_\odot$)	1.19 ± 0.06
R_* (R$_\odot$)	1.22 ± 0.06
$\log g_*$ (cgs)	4.34 ± 0.05
ρ_* ($\rho_\odot$)	0.65 ± 0.10
M_P (M$_{\text{Jup}}$)	0.101 ± 0.005
R_P (R$_{\text{Jup}}$)	0.63 ± 0.03
$\log g_P$ (cgs)	2.77 ± 0.05
ρ_P (ρ_J)	0.41 ± 0.07
λ (deg)†	3 ± 5
$v\sin i$ (km s^{-1})	5.1 ± 0.3
a (au)	0.0641 ± 0.0011
Irradiation (W m^{-2})	$6.0 \pm 0.6 \times 10^5$
$T_{P, A = 0}$ (K)	1270 ± 30

Notes: Priors were $M_* = 1.18 \pm 0.03$ M$_\odot$ and $R_* = 1.23 \pm 0.06$ R$_\odot$ Errors are 1σ; Limb-darkening coefficients were:
r band: a1 = 0.512, a2 = 0.337, a3 = −0.138, a4 = −0.015
I band: a1 = 0.579, a2 = 0.039, a3 = 0.104, a4 = −0.101
z band: a1 = 0.599, a2 = −0.076, a3 = 0.191, a4 = −0.131

According to *Gaia* DR2 (Gaia Collaboration 2018), WASP-166 has a relatively high proper motion of 56 mas yr^{-1}, which at the DR2 distance gives a transverse velocity of 30.0 $\pm$ 0.3 km s^{-1}, which complements the DR2 radial velocity of 24.0 $\pm$ 0.4 km s^{-1}. WASP-166 is relatively isolated, with the nearest DR2 star being 8 arcsec away and 9 mag fainter. There is no excess astrometric noise reported (such noise can indicate an unresolved binary).

4 SYSTEM ANALYSIS

As is standard for WASP discovery papers, we combined the photometry and RV data sets into a Markov-chain Monte Carlo (MCMC) analysis (e.g. Collier Cameron et al. 2007). This fits parameters including T_c (the epoch of mid-transit), P (the orbital period), ΔF (the transit depth that would be observed in the absence
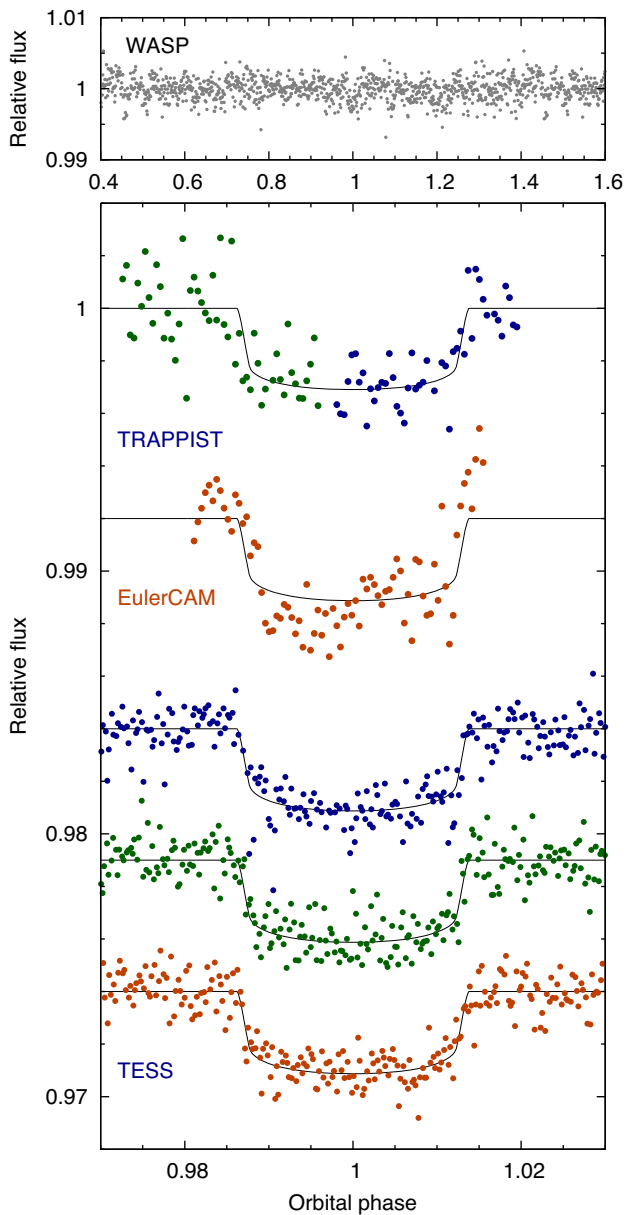
Figure 1. WASP-166b photometry: (Top) The WASP data folded on the transit period. (Main panel) Photometry from TRAPPIST-South, Euler-CAM, and the three TESS transits, together with the fitted MCMC model (the TRAPPIST ingress, green points, and egress, blue points, are from different transits but are shown together).

of limb darkening), T_{14} (duration from first to fourth contact), b (the impact parameter), and K_1 (the stellar reflex velocity). For fitting the photometry we adopted the four-parameter, non-linear limb darkening of Claret (2000), interpolating coefficients for the appropriate stellar temperature and metallicity.

We allowed for RV offsets between different data sets, treating the CORALIE data before and after a 2014 November upgrade, the HARPS data round the orbit, and the three HARPS transit observations, all as independent sets (the RV values are listed in Table A1). The γ velocity of the system given in Table 2 is that for the 27 HARPS data points around the orbit.

We adopted a zero-eccentricity fit for WASP-166b, as is usually the case for lower mass, short-period planets. It is clear, though, that
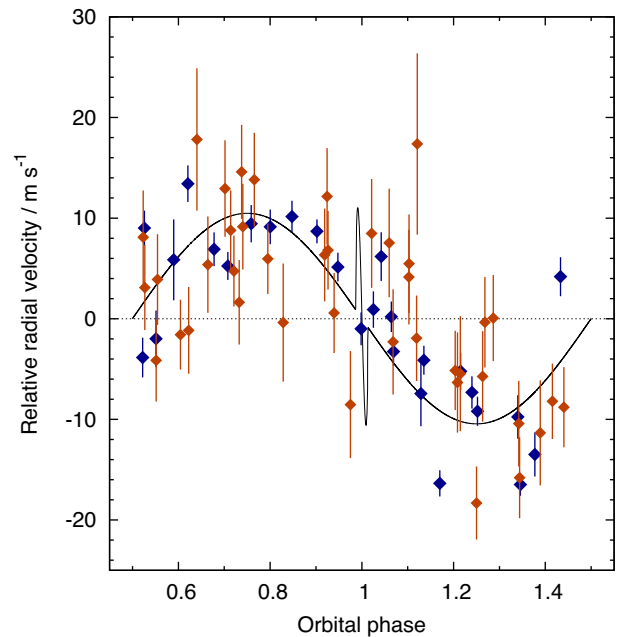
Figure 2. The HARPS (blue) and CORALIE (orange) radial velocities and fitted orbital model (the HARPS data in Fig. 4 are not shown here for clarity).
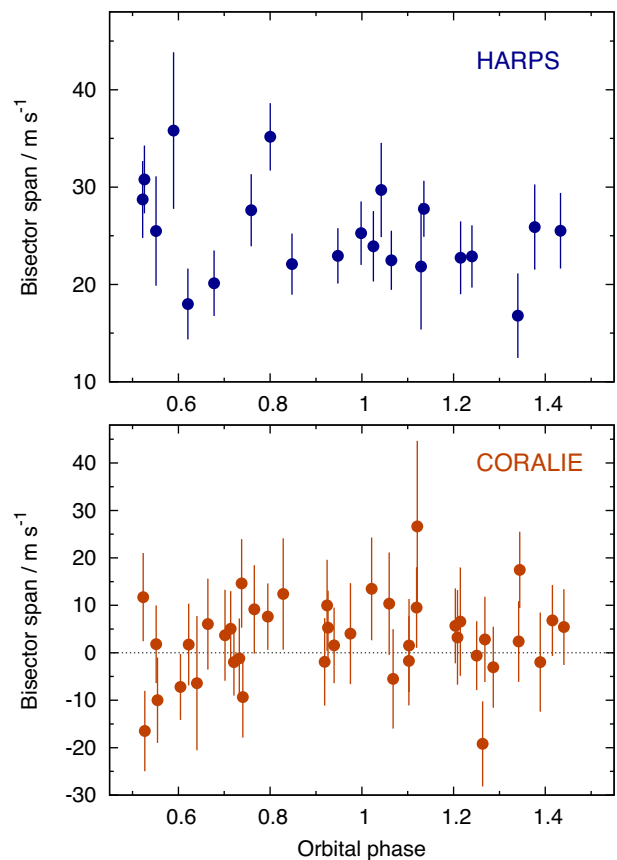

Figure 3. The spectroscopic bisector spans against orbital phase. The HARPS and CORALIE data are plotted separately since their accuracy is different. The absence of any correlation with radial velocity is a check against transit mimics.
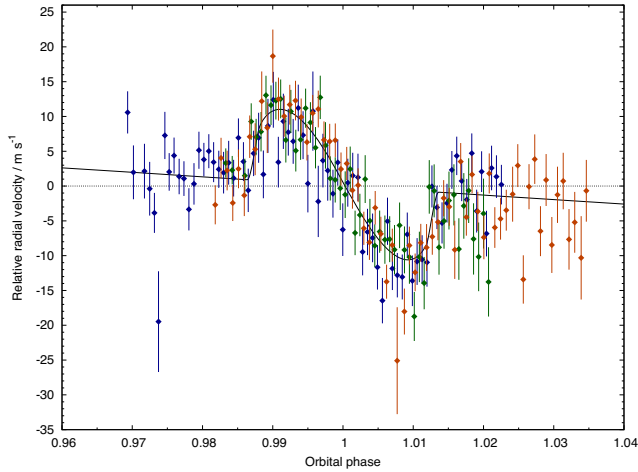
Figure 4. HARPS RV data through transit along with the fitted R–M model. The colours denote data from different nights (blue: 2017-01-14; green 2017-03-04; orange 2017-03-15).
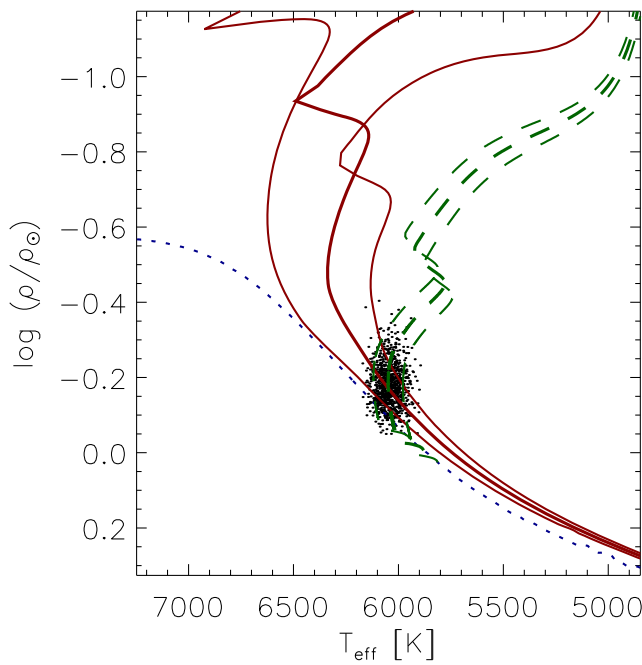

Figure 5. The host star's effective temperature (T_{eff}) versus density (where the dots are outputs of the BAGEMASS MCMC). The blue dotted line is the zero-age main sequence, the green dashed lines are the evolutionary tracks (for the best-fitting mass of 1.18 $M_\odot$ and error bounds of 0.03 $M_\odot$), while the red lines are isochrones (for the best-fitting age of 2.1 Gyr and error bars of 0.9 Gyr).

there are additional RV deviations from the fitted model; indeed the fit to the HARPS RVs around the orbit has a χ^2 of 217 for 27 data points. Allowing an eccentric solution did not significantly improve the fit (producing a non-significant value of $e = 0.03 \pm 0.02$, with a 2σ upper limit of 0.07), nor did allowing a long-term drift in the RVs. Adding a second sinusoid, as could be caused by a second planet, also failed to model the additional variability, which tells us that it is not a coherent modulation.

The MCMC process accounts for the additional RV variability, and indeed any red noise in the transit light curves, by inflating each
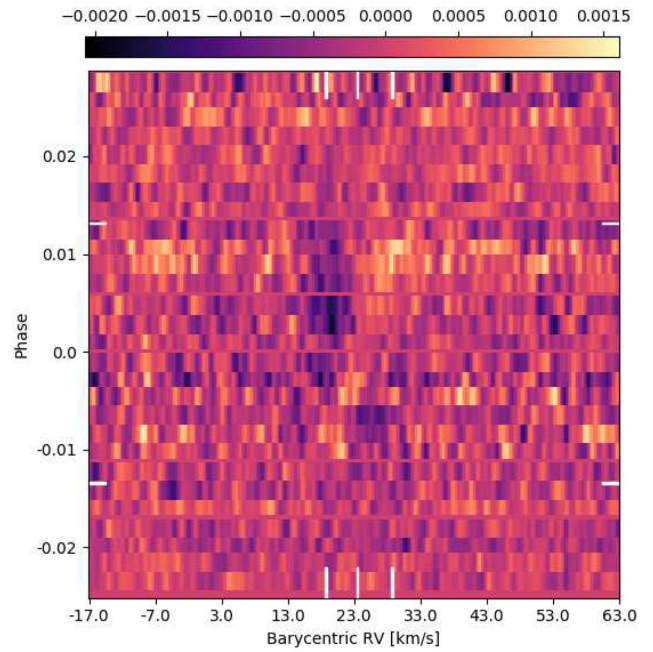

Figure 6. The line profiles through transit. The white lines show (x-axis) the mean γ velocity of the system and the $v\sin i$ line width, and (y-axis) the beginning and end of transit. The Doppler shadow of the planet moves from blue to red over the transit. The mean profile has been subtracted, resulting in a reduced level elsewhere in transit.
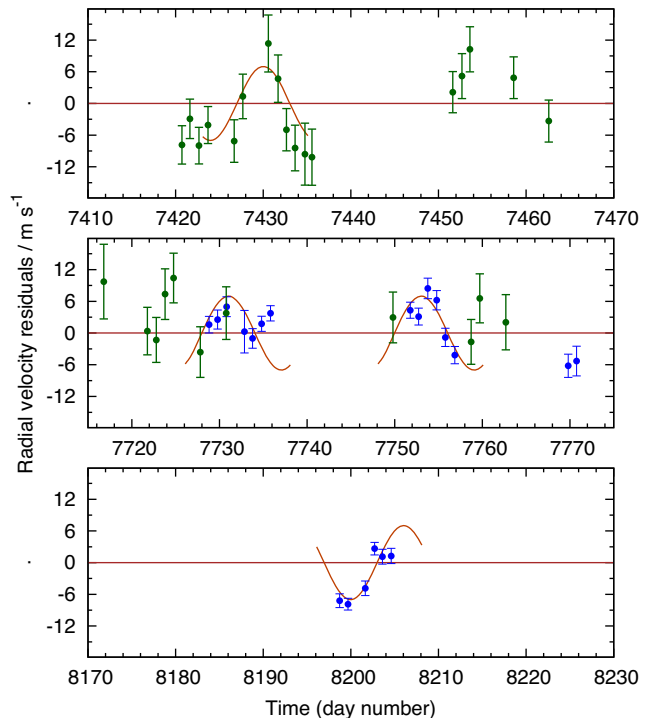

Figure 7. The residuals of the RV data to the orbital model, plotted as a function of time. The blue and green symbols are HARPS and CORALIE data, respectively. The red line shows portions of sinusoid (not phase coherent) that illustrate the putative 12.1-d stellar rotation period.
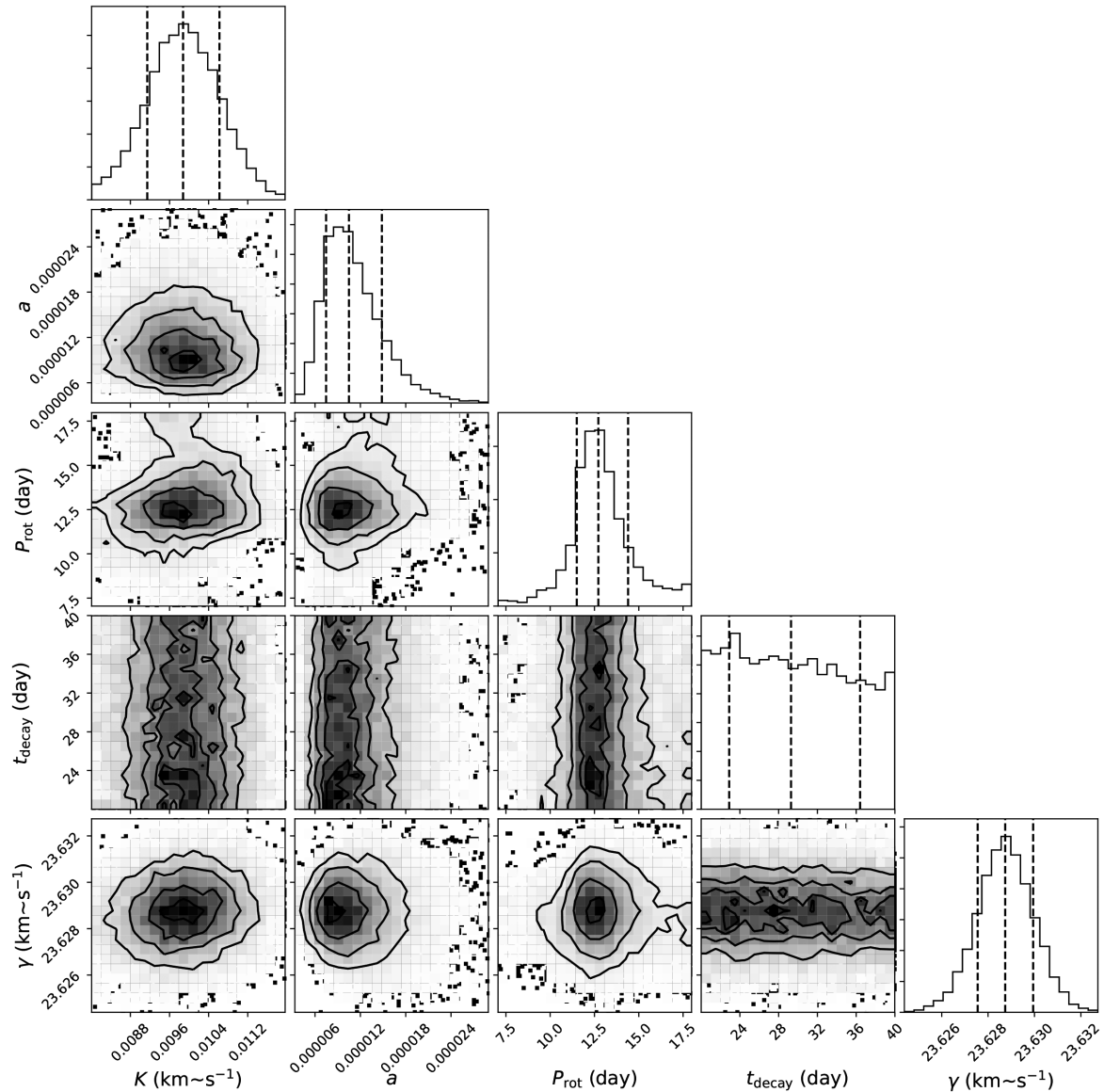
Figure 8. Parameter distributions from the Gaussian-process analysis of the correlated RV residuals. The decay time-scale t_{decay} is not constrained by the data, but there is a clear preference for a rotational period, $P_{rot} = 12.3 \pm 1.9$ d.

data set's errors to give $\chi^2_\nu = 1$; this balances the different data sets' influence on the final result and inflates the errors on the output parameters.

As is usual in WASP discovery papers we also constrained the stellar mass by adopting a prior based on the measured effective temperature and metallicity values, together with the stellar density obtained by an initial fit to the transit. For this we used the BAGEMASS code described in Maxted, Serenelli & Southworth (2015). This resulted in a mass estimate of 1.18 ± 0.03 M$_\odot$, and also an age estimate of 2.1 ± 0.9 Gyr. The measured lithium abundance is consistent with this age estimate, though does not constrain the age further.

Lastly, we include a constraint on the stellar radius derived from *Gaia* DR2 (Gaia Collaboration 2018). The DR2 parallax of 8.730 ± 0.045 mas implies a distance of 113 ± 1 pc (where we have applied the correction suggested by Stassun & Torres 2018). Using the infrared flux method (Blackwell & Shallis 1977) this implies a stellar radius of 1.23 ± 0.06 R$_\odot$, which we adopt as a prior.

The initial version of this paper lacked the TESS data and so, with only limited photometry, the parameters were less secure. However, the *Gaia* input tied down the stellar radius, and hence the impact parameter, and thus, after including the TESS data, the values have changed by less than an error bar.

The adopted system parameters are listed in Table 2, while the data and fit are shown in Figs 1–4. We also show a modified H–R diagram for the star in Fig. 5.

4.1 The Rossiter–McLaughlin effect

The above MCMC fit included fitting the in-transit radial velocities, where we use the parametrization of Hirano et al. (2011) to model the RV deviations caused by the Rossiter–McLaughlin effect (Fig. 4). Any differences between the data on the three different nights of data could be caused by the planet crossing starspots or faculae regions.
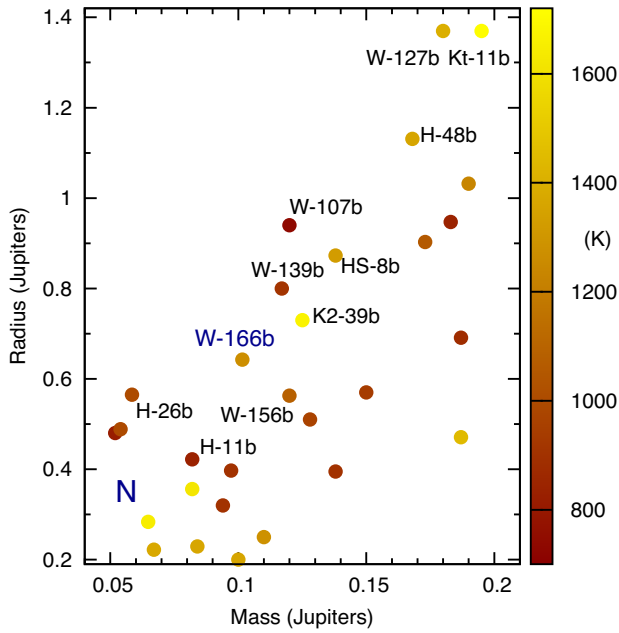
Figure 9. Masses and radii of transiting 'hot' super-Neptune planets (with orbital periods < 10 d). The symbols are coloured according to the planet's equilibrium temperature. The labelled planets are WASP-107b (Anderson et al. 2017), WASP-127b (Lam et al. 2017), WASP-139b (Hellier et al. 2017), WASP-156b (Demangeon et al. 2018), HAT-P-11b (Bakos et al. 2010), HAT-P-26b (Hartman et al. 2011), HAT-P-48b (Bakos et al. 2016), HATS-8b (Bayliss et al. 2015), KELT-11b (Pepper et al. 2017), and K2-39b (Van Eylen et al. 2016; Petigura et al. 2017). The location of Neptune is marked with an N.

The sky-projected obliquity angle, λ, is measured as 3 ± 5 deg, and thus the planet's orbit is aligned with the stellar rotation. The fitted $v\sin i$ of 5.1 ± 0.3 km s^{-1} is consistent with the spectroscopic value of 4.6 ± 0.8 km s^{-1}.

In Fig. 6 we show the HARPS line profiles through transit, in a tomographic display following the methods in Temple et al. (2018). This figure shows the averaged data from all three transits, with the mean profile subtracted to better show variations. The planet trace can be seen moving prograde from blue to red over the transit. Fitting the tomogram directly (e.g. Temple et al. 2018), as opposed to fitting the modelled RVs, produces parameters consistent with those in Table 2, where again the uncertainties are currently dominated by the quality of the photometry.

4.2 Possible magnetic activity

The RV data clearly show deviations about the orbital model (Fig. 2). To illustrate this we plot in Fig. 7 some of the residual RV values as a function of time (omitting the in-transit R–M sequences). The residuals appear to be correlated from night to night.

Given the transit and the fact that the planet's orbit is aligned we can presume that the stellar rotation axis is perpendicular to the line of sight, and thus combining the $v\sin i$ fitted to the R–M effect with the fitted stellar radius we obtain a rotational period of 12.1 ± 0.9 d. To guide the eye we plot in Fig. 7 portions of 12.1-d sinusoid (amplitude 7 m s^{-1}), and conclude that the RV deviations might result from magnetic activity.

We have also investigated the variability by modelling the HARPS RVs using a Gaussian-process (GP) analysis following the method detailed in Haywood et al. (2014). To model the residuals, this adds to the orbital motion three hyperparameters (with uniform
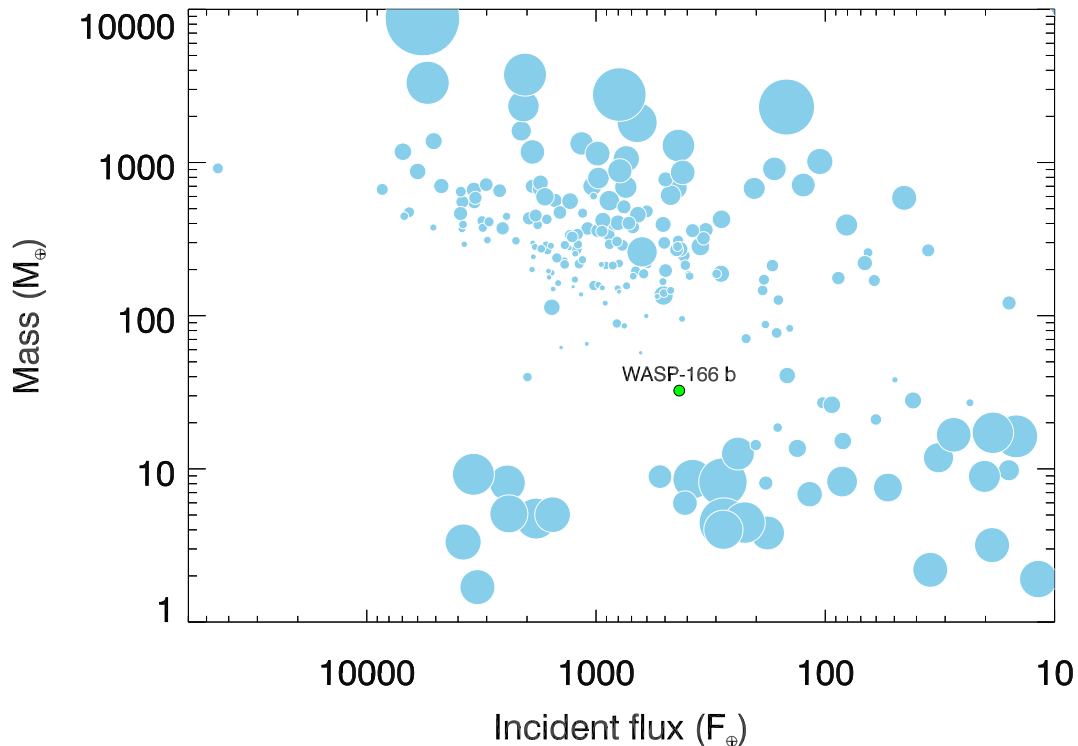

Figure 10. Exoplanet mass versus incident flux, showing the location of WASP-166b in the 'sub-Jovian desert'. The symbol area is proportional to the bulk density of the planet. We include only planets with host stars brighter than $V = 12$. Data are from http://exoplanets.org/.
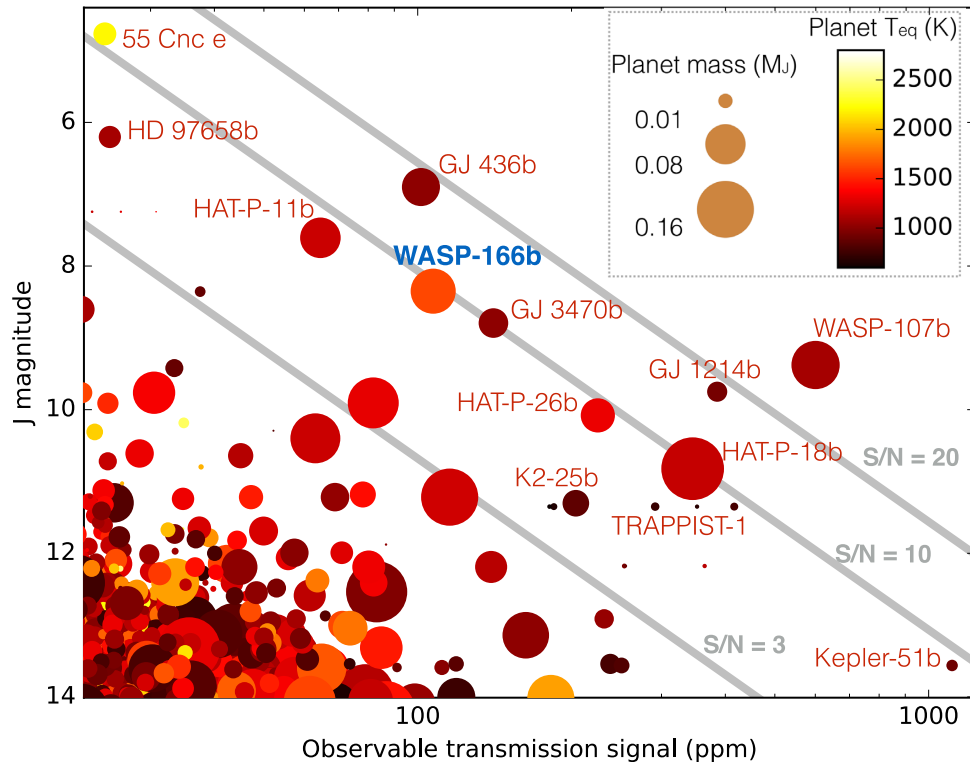
Figure 11. An illustration of prime low-mass planets ($<0.2\ M_{\rm Jup}$) for atmospheric characterization, based on the scale height of the atmosphere, the transit depth, and the host-star brightness.

priors), namely an amplitude a, a period $P_{\rm rot}$ (taken to be the rotational period), and an exponential decay time-scale, $t_{\rm decay}$ (being the time-scale on which magnetic activity would lose coherence). We set the last to ~ 30 d, which is physically realistic, but is not constrained by the data since we have few observations separated by that time-scale. The 'corner plot' of the GP output is shown in Fig. 8.

The analysis produces a clear preference for a rotational period of 12.3 ± 1.9 d, consistent with that from the R–M $v\sin i$, and in line with the magnetic-activity hypothesis. The resulting values of $K_1 = 0.0100 \pm 0.0006\ {\rm km\,s^{-1}}$ and $\gamma = 23.6288 \pm 0.0012\ {\rm km\,s^{-1}}$ are consistent with those in Table 2.

Having found evidence of a 12-d rotational period we then searched the WASP light curve for any rotational modulation, using the methods of Maxted et al. (2011). The WASP data amount to 33 000 data points spanning ~ 150 nights of coverage in each of six consecutive seasons from 2007 to 2012. We found no significant modulation to a 95 per cent limit of 1 mmag. Given the lack of a photometric modulation, the correlated RV residuals might be attributable to magnetic suppression of photospheric convection in spot-free facular active regions (e.g. Milbourne et al. 2019).

5 DISCUSSION

With a mass of 1.9 Neptunes, WASP-166b is the lowest mass planet yet discovered by the WASP survey. It also has a bloated radius of $0.63 \pm 0.03\ R_{\rm Jup}$. The 'super-Neptune' region of the mass–radius diagram for known, short-period transiting exoplanets is plotted in Fig. 9, showing that WASP-166b is near the upper size bound for a planet of its mass. The empirically observed upper bound (from WASP-127b to WASP-107b to HAT-P-26b) is falling rapidly

in this mass range, which may be telling us about radius-inflation mechanisms and the ability of a lower mass planet to hold on to its envelope under the effects of irradiation.

For example, Mazeh et al. (2016) have shown that there is a 'Neptune desert' at short orbital periods, with almost no hot-Neptune planets at periods <5 d and fewer at periods <10 d, when compared to abundant hot Jupiters and super-Earths (see also Thorngren & Fortney 2018 on the lack of inflated sub-Saturns). To illustrate the 'Neptune' or 'sub-Jovian desert' we highlight the location of WASP-166b on a plot of planet mass against insolation (Fig. 10).

The desert is likely the result of photoirradiation of inwardly migrating planets (e.g. Owen & Lai 2018; Sestovic, Demory & Queloz 2018; Szabó & Kálmán 2019). Jupiter-mass planets are able to resist photoevaporation, and continue to migrate inwards by tidal orbital decay, whereas a low-surface-gravity Neptune such as WASP-166b could not. A hot Neptune could instead be captured into a short-period orbit from a high-eccentricity-migration pathway, and so, being new to its orbit, would not have undergone the photoevaporation that would have occurred had it migrated there by the slower process of orbital decay. However, such capture only occurs for a narrow range of parameter space (Owen & Lai 2018), and so such systems would be rare.

With a period of 5.4 d and orbiting an F star, WASP-166b has a relatively high irradiation of $6 \times 10^5\ {\rm W\,m^{-2}}$ (440 times Earth's insolation) for such a low-surface-gravity planet. Thus it appears to be a rare object, with a radius bloated by irradiation, on the boundary of the Neptune desert.

The Rossiter–McLaughlin observations show that the orbit is aligned ($\lambda = 3 \pm 5$ deg). This is consistent with it being on a lengthy inwardly migration, during which it has become bloated owing to irradiation. However, recent capture from high-eccentricity

pathways can also produce aligned orbits, so this is not conclusive. Relatively few of the super-Neptune planets in Fig. 9 have had obliquity angles measured, though those that have – HAT-P-11b (Bakos et al. 2010; Winn et al. 2010), WASP-107b (Anderson et al. 2017; Dai & Winn 2017; Močnik et al. 2017) and GJ 436b (Gillon et al. 2007; Bourrier et al. 2018) – are all known to be misaligned.

The bloated nature of WASP-166b combines with a bright host star of $V = 9.36$ to make it a prime target for atmospheric characterization. Indeed, recent observations of irradiated low-surface-gravity planets show indications of photoevaporating atmospheres (e.g. Mansfield et al. 2018; Spake et al. 2018). The expected signal for a transmission spectrum depends on the atmospheric scale height, transit depth, and host-star magnitude (e.g. equation 36 of Winn 2010). In Fig. 11 we compare the signal expected for WASP-166b with other low-mass planets ($M < 0.2\,M_{\rm Jup}$). This shows that WASP-166b is likely to be among the best targets for such studies, though this may be more difficult if the star is indeed magnetically active, as indicated by correlated deviations in the RV data. We suggest that WASP-166b is potentially a prime target for the *James Webb Space Telescope*, and that it should first be observed with *HST* in order to assess the cloudiness of its atmosphere.

REFERENCES

Anderson D. R. et al., 2017, A&A, 604, A110
Bakos G. Á. et al., 2010, ApJ, 710, 1724
Bakos G. Á. et al., 2016, preprint (arXiv:1606.04556)
Bayliss D. et al., 2015, AJ, 150, 49
Blackwell D. E., Shallis M. J., 1977, MNRAS, 180, 177
Bourrier V. et al., 2018, Nature, 553, 477
Chen G. et al., 2018, A&A, 616, A145
Claret A., 2000, A&A, 363, 1081
Collier Cameron A. et al., 2007, MNRAS, 375, 951
Dai F., Winn J. N., 2017, AJ, 153, 205
Demangeon O. D. S. et al., 2018, A&A, 610, A63
Doyle A. P. et al., 2013, MNRAS, 428, 3164
Doyle A. P., Davies G. R., Smalley B., Chaplin W. J., Elsworth Y., 2014, MNRAS, 444, 3592
Gaia Collaboration, 2018, A&A, 616, A1
Gillon M. et al., 2007, A&A, 472, L13
Gillon M. et al., 2013, A&A, 552, A82
Hartman J. D. et al., 2011, ApJ, 728, 138
Haywood R. D. et al., 2014, MNRAS, 443, 2517
Hellier C. et al., 2017, MNRAS, 465, 3693
Hellier C. et al., 2018, MNRAS
Hirano T., Suto Y., Winn J. N., Taruya A., Narita N., Albrecht S., Sato B., 2011, ApJ, 742, 69
Kreidberg L., Line M. R., Thorngren D., Morley C. V., Stevenson K. B., 2018, ApJ, 858, L6
Lam K. W. F. et al., 2017, A&A, 599, A3
Lendl M. et al., 2012, A&A, 544, A72
Mansfield M. et al., 2018, ApJ, 868, L34
Maxted P. F. L. et al., 2011, PASP, 123, 547
Maxted P. F. L., Serenelli A. M., Southworth J., 2015, A&A, 575, A36
Mazeh T., Holczer T., Faigler S., 2016, A&A, 589, A75
Milbourne T. W. et al., 2019, ApJ, 874, 107
Močnik T., Hellier C., Anderson D. R., Clark B. J. M., Southworth J., 2017, MNRAS, 469, 1622
Owen J. E., Lai D., 2018, MNRAS, 479, 5012
Palle E. et al., 2017, A&A, 602, L15
Pepper J. et al., 2017, AJ, 153, 215
Petigura E. A. et al., 2017, AJ, 153, 142
Pollacco D. L. et al., 2006, PASP, 118, 1407
Ricker G. R. et al., 2016, in MacEwen H. A., Fazio G. G., Lystrup M., Batalha N., Siegler N., Tong E. C., eds, Proc. SPIE Conf. Ser. Vol. 9904, Space Telescopes and Instrumentation 2016: Optical, Infrared, and Millimeter Wave. SPIE, Bellingham, p. 99042B
Rickman E. L. et al., 2019, A&A, 625, A71
Sestovic M., Demory B.-O., Queloz D., 2018, A&A, 616, A76
Spake J. J. et al., 2018, Nature, 557, 68
Stassun K. G., Torres G., 2018, ApJ, 862, 61
Szabó G. M., Kálmán S., 2019, MNRAS, 485, L116
Temple L. Y. et al., 2018, MNRAS, 480, 5307
Thorngren D. P., Fortney J. J., 2018, AJ, 155, 214
Triaud A. H. M. J. et al., 2013, A&A, 551, A80
Udry S. et al., 2019, A&A, 622, A37
Van Eylen V. et al., 2016, AJ, 152, 143
Winn J. N., 2010, preprint, (arXiv:1001.2010)
Winn J. N. et al., 2010, ApJ, 723, L223

SUPPORTING INFORMATION

Supplementary data are available at *MNRAS* online.

Table A1. WASP-166 radial velocities.

Please note: Oxford University Press is not responsible for the content or functionality of any supporting materials supplied by the authors. Any queries (other than missing material) should be directed to the corresponding author for the article.

APPENDIX A:

Table A1. WASP-166 radial velocities. (The complete table is available online.)

BJD − 2400000 (UTC)	RV (km s^{-1})	σ_{RV} (km s^{-1})	Bisector (km s^{-1})
CORALIE:			
56715.69870	23.60674	0.00420	− 0.00118
56718.61401	23.60476	0.00449	0.00282
57186.46596	23.59798	0.00571	0.00657
57189.46427	23.61726	0.00466	0.00915
57379.74611	23.60818	0.00352	− 0.00198
57420.73070	23.58513	0.00363	− 0.00060
57421.63091	23.59524	0.00374	0.00681
57422.66015	23.60186	0.00347	− 0.00721
57423.69579	23.60940	0.00350	0.00762

Note: Bisector errors are twice RV errors. Lines denote an instrument upgrade, or separate through-transit sequences.

This paper has been typeset from a TEX/LATEX file prepared by the author.